Molecular Plant • Volume 3 • Number 5 • Pages 818–833 • September 2010 RESEARCH ARTICLE

Virus-Induced Gene Silencing Offers a Functional Genomics Platform for Studying Plant Cell Wall Formation

Xiaohong Zhu[a], Sivakumar Pattathil[b], Koushik Mazumder[b], Amanda Brehm[b], Michael G. Hahn[b,c], S.P. Dinesh-Kumar[d] and **Chandrashekhar P. Joshi[a,e,1]**

a Biotechnology Research Center, School of Forest Resources and Environmental Science, Michigan Technological University, Houghton, MI 49931, USA
b BioEnergy Science Center, Complex Carbohydrate Research Center, University of Georgia, 315 Riverbend Road, Athens, GA 30602, USA
c Department of Plant Biology, University of Georgia, Athens, GA 30602, USA
d Section of Plant Biology and Genome Center, University of California, Davis, CA 95616, USA
e Department of Bioenergy Science and Technology, Chonnam National University, Gwangju 500–757, Korea

ABSTRACT Virus-induced gene silencing (VIGS) is a powerful genetic tool for rapid assessment of plant gene functions in the post-genomic era. Here, we successfully implemented a Tobacco Rattle Virus (TRV)-based VIGS system to study functions of genes involved in either primary or secondary cell wall formation in *Nicotiana benthamiana* plants. A 3-week post-VIGS time frame is sufficient to observe phenotypic alterations in the anatomical structure of stems and chemical composition of the primary and secondary cell walls. We used cell wall glycan-directed monoclonal antibodies to demonstrate that alteration of cell wall polymer synthesis during the secondary growth phase of VIGS plants has profound effects on the extractability of components from woody stem cell walls. Therefore, TRV-based VIGS together with cell wall component profiling methods provide a high-throughput gene discovery platform for studying plant cell wall formation from a bioenergy perspective.

Key words: Plant cell wall; VIGS; cellulose; xylan; lignin; Nicotiana.

INTRODUCTION

Plant cells develop two types of walls: primary and secondary cell walls (Cosgrove, 2005). The formation of primary walls accompanies cell division and expansion where deposition of polysaccharides and structural proteins occurs outside the plasma membrane. The dynamic structure and composition of the primary wall determine cell shape while controlling the rate and direction of cell growth. The secondary wall consists of multiple layers of polysaccharides and polyphenolics deposited between the primary cell wall and plasma membrane after the cell ceases to expand. The relatively rigid structure of the secondary wall provides the plant with mechanical strength and serves as a physical barrier against pathogen attack (Lagaert et al., 2009). Moreover, primary and secondary cell walls are the major carbon-containing components in biomass (Pauly and Keegstra, 2008; Sandhu et al., 2009). Despite our knowledge of their crucial roles, we still lack mechanistic insights into the processes of cell wall formation. The structural complexity of the cell wall implies that a large number of genes may be involved in its biogenesis (Mohnen et al., 2008) and that their expression is orchestrated specifically in different cell types, tissues or organs, and species in response to developmental and environmental cues (Farrokhi et al., 2006).

Based on analyses of the available genome sequences of *Arabidopsis*, rice, and poplar, a number of genes have been annotated as having either known or unknown functions in cell wall formation (Aspeborg et al., 2005; Yong et al., 2005). Large collections of ESTs relevant to cell wall synthesis and wood formation have also been generated in poplar and other economically valuable tree species (Sterky et al., 1998, 2004). Furthermore, microarray profiling and co-expression analysis have led to the identification of numerous candidate genes potentially involved in cell wall synthesis (Brown et al., 2005; Persson et al., 2005). A system that enables rapid determination of the biological functions of genes involved in cell wall formation is necessitated by recent advances in genomic data collections.

[1] To whom correspondence should be addressed. E-mail cpjoshi@mtu.edu.

© The Author 2010. Published by the Molecular Plant Shanghai Editorial Office in association with Oxford University Press on behalf of CSPP and IPPE, SIBS, CAS.

doi: 10.1093/mp/ssq023, Advance Access publication 3 June 2010
Received 5 February 2010; accepted 24 April 2010

Downloaded from mplant.oxfordjournals.org at Oak Ridge National Lab/UT-Battelle on September 14, 2011

Considerable progress in understanding of cell wall formation has been made using *Arabidopsis* (Somerville, 2006). However, this system has limitations for increasing our understanding of wood formation, which involves massive secondary growth that does not typically occur in *Arabidopsis* (Sterky et al., 1998). *Nicotiana benthamiana*, a close relative of common tobacco (*N. tabacum*) that possesses the ability to undergo secondary growth, provides a potential model species for cell wall studies. In addition, availability of the tobacco genome sequence (www.pngg.org/tgi/) will facilitate novel gene discovery in cell wall formation in this plant model system. Most importantly, *N. benthamiana* is an excellent well proven platform for Virus Induced Gene Silencing (VIGS). VIGS, a transient RNAi-mediated gene silencing approach, facilitates rapid gene function assessment without the requirement of generating stable transgenics (Burch-Smith et al., 2004). VIGS has been successfully used to address biological questions related to plant defense, development, and metabolism in many plant species (Lu et al., 2003; Burch-Smith et al., 2004; Robertson, 2004).

A potato virus X (PVX)-based VIGS has been used to silence a cellulose synthase (CesA) gene in *N. benthamiana* plants to assess its function in primary cell wall formation (Burton et al., 2000). PVX-*NtCesA-1* infected plants showed a cellulose-deficient phenotype and alterations in leaf and whole-plant morphology. This study highlighted the specificity of VIGS for the functional analysis of cell wall synthesis genes because VIGS of two highly similar (80% homology) CesA genes produced completely different phenotypes. Here, we have optimized tobacco rattle virus (TRV)-based VIGS (Liu et al., 2002) in *N. benthamiana* plants as a rapid, reliable, and robust system to assess gene function in cell wall formation. We demonstrate that TRV-VIGS together with comprehensive microarray polymer profiling (CoMPP) assay (Moller et al., 2007) and glycome profiling using cell wall glycan-directed monoclonal antibody-ELISA (enzyme-linked immunosorbent assay) (Pattathil et al., 2010) serve as a genome-wide high-throughput gene discovery platform in lignocellulosic biomass synthesis.

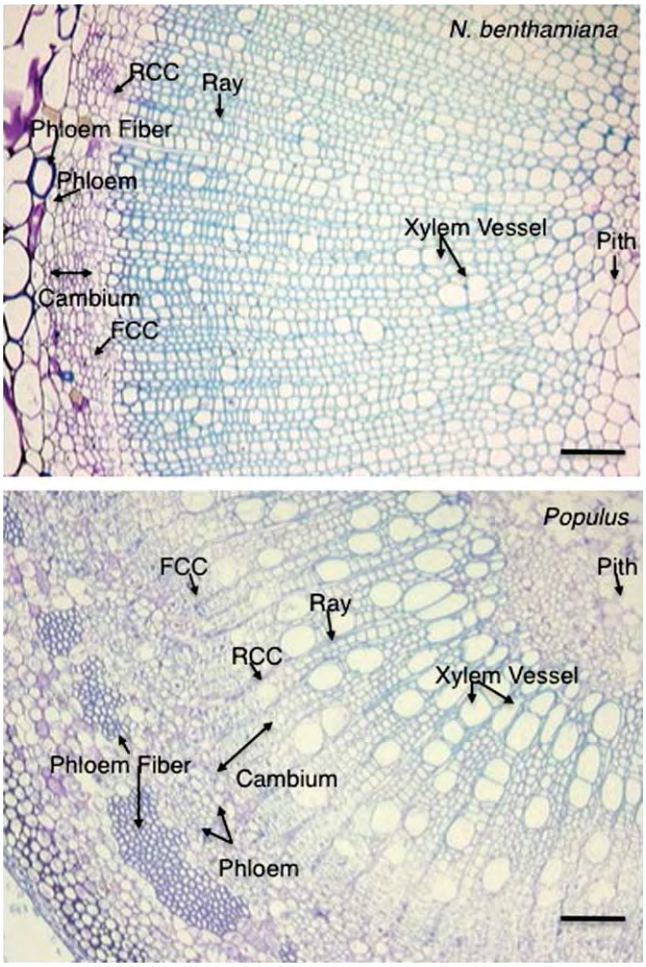

Figure 1. Comparison of Stem Structures of *N. benthamiana* and *Populus.*

Various structuralelements of the stem in TBO-stained transverse sections of 14th internodes of *N. benthamiana* (top panel) and *Populus* (bottom panel) are indicated by arrows. FCC, fusiform cambial cells (FCC); RCC, radial ray cambial cells. Scale bar represents 100 μm.

RESULTS

N. benthamiana Stems Are Similar to Poplar Woody Stems

To determine whether the mature stems of *N. benthamiana* possess anatomical characteristics similar to woody stem, we compared *N. benthamiana* and poplar stem structures. Transverse sections (TS) of the 14th internode of 6-week-old *N. benthamiana* and 8-week-old poplar show a similar secondary xylem structure (Figure 1). Phloem, cambium zone, xylem vessels, and rays are well distinguished in TS of *N. benthamiana* stems. Xylem vessels are small, solitary, and arranged in small groups in *N. benthamiana.* In poplar, large xylem vessels are seen in long radial multiples (Figure 1). In *N. benthamiana*, the vascular cambium is visible in TS as a layer five to six cells thick between the secondary xylem and phloem. Two types of initials were clearly distinguishable in the vascular cambium zone, the axially elongated fusiform cambial cells (FCC), and the radial ray cambial cells (RCC). Radial rays derived from RCC are an important determinant for horizontal secondary growth (Mellerowicz et al., 2001; Baucher et al., 2007). In both *N. benthamiana* and poplar stems, radial ray cells are arranged in a uniseriate band (Figure 1). However, in poplar, radial rays occur at high frequency and appear to be evenly distributed within secondary xylem. In both *N. benthamiana* and poplar, xylem parenchyma cells are organized in radial strands and are scattered. *N. benthamiana* and poplar phloem appear different in TS (Figure 1). Unlike poplar, in which phloem fiber cells form groups, they are relatively scattered as individual cells in *N. benthamiana.* Collectively, these data suggest that *N. benthamiana* plant stems possess most of the structural characteristics of poplar woody stems.

Downloaded from mplant.oxfordjournals.org at Oak Ridge National Lab/UT-Battelle on September 14, 2011

Deposition of Cellulose, Hemicellulose, and Lignin in *N. benthamiana* Stems

To establish a framework for studying cell wall formation using TRV-based VIGS in *N. benthamiana*, we analyzed the deposition of three major cell wall macromolecules, cellulose, xylan, and lignin in the first to seventh internodes of 3 weeks post infiltration (wpi) VIGS plants. The first through the seventh internodes in *N. benthamiana* stems encompass the developmental stages that cover the transition from primary to secondary stem growth. To monitor crystalline cellulose deposition in primary and secondary cell walls, we labeled stem cell walls using CBM3a (see Methods), a carbohydrate-binding module derived from the scaffolding protein of the *Clostridium thermocellum* cellulosome that binds primarily to crystalline cellulose (Blake et al., 2006). We observed strong labeling in xylem, phloem, cortex, and pith cells, but relatively weak signals in undifferentiated cambium cells (Figure 2A), suggesting that increased deposition of crystalline cellulose occurs in xylem vessels as secondary xylem cells differentiate and mature. To detect xylan deposition, we used the LM10 monoclonal antibody that is known to bind to less branched (1–4)-β-D-xylans (McCartney et al., 2005). We observed LM10-labeled xylan only in secondary cell wall-containing xylem vessels and phloem fiber cells (Figure 2B). Moreover, LM10-labeled phloem fiber cells appear only in TS of the sixth and seventh internodes. Several layers of unlignified cells near the cambial zone showed stronger labeling compared to the lignified xylem cells, suggesting that fluorescence in the probed cells was partially quenched by lignin (Figure 2B–2D, 6–7). To monitor lignin deposition, we followed UV-induced autofluorescence. A strong autofluorescence signal was observed in the secondary xylem tissues of UV-illuminated TS of the sixth and seventh internodes (Figure 2C and 2D), which indicates that there is a clear transition from primary growth to secondary growth between internodes 5 and 6. The sequential deposition of cellulose, xylan, and lignin observed in this study (Figure 2A–2C) clearly indicates that in secondary cell walls, xylans are deposited only after crystalline cellulose formation, but before cell walls are lignified. Like woody stems, lignification first starts in vessel cells, whereas fiber cells are lignified later (Mellerowicz et al., 2001).

Together, our results demonstrate that *N. benthamiana* stems have characteristics that are similar to those of woody stems. Three major cell wall macromolecules are sequentially deposited within the xylem cell wall in the same manner as occurs during the maturation of secondary xylem in the woody stems. Thus, the seventh internode of 3-wpi VIGS plants possesses the mature secondary xylem cells that would be useful for examining structural and compositional phenotypes of VIGS plants.

VIGS-Mediated Silencing of Genes Involved in Cellulose, Xylan, and Lignin Synthesis

To investigate whether TRV-based VIGS is effective for studying cellulose, xylan, and lignin synthesis in *N. benthamiana* stem cell walls, we targeted cellulose-, xylan- and lignin-related genes, which were chosen based on their sequence homology with corresponding *Arabidopsis* genes (Supplemental Table 1). *NbCesA6* and *NbCesA8* are two orthologs of *AtCesA6* (AT5G64740) and *AtCesA8* (AT4G18780), which are known to be involved in primary and secondary cell wall cellulose synthesis, respectively (Fagard et al., 2000; Taylor et al., 2000). *NbCOBRA* is an ortholog of *AtCOBRA* (AT5G60920) that was previously shown to control cell expansion by orientating cellulose microfibril deposition in *Arabidopsis* (Schindelman et al., 2001; Roudier et al., 2005). VIGS-*NbCesA6*, VIGS-*NbCesA8*, and VIGS-*NbCOBRA*-infected plants were shorter in stature than VIGS-vector-infected control plants at 3 wpi. However, VIGS-*NbCOBRA*-infected plants were severely dwarfed (Figure 3B, panel 1). The fourth pair of leaves from the top of VIGS-*NbCesA8*-infected plants was small and curled, while that of VIGS-*NbCesA6* and VIGS-*NbCOBRA*-infected plants were small, flat, and lumpy compared to control plants (Figure 3A, panel 1). The leaf phenotype of VIGS-*NbCesA6* appeared very similar to those described in a previous report, in which the leaves of *Nt-CesA-1*-silenced plants had a crunchy texture and lumpy surfaces (Burton et al., 2000). The small, dark-green, and curled leaves of VIGS-*NbCesA8*-infected plants suggest that down-regulation of secondary wall CesA may affect the leaf development by causing defective development of leaf vascular bundles, leading to the curled leaf shape. Although most of the published *Arabidopsis* COBRA work focused on its effect on roots (Roudier et al., 2005), our results show that silencing of *NbCOBRA* results in dramatic growth reduction of aerial parts of the plant. The observed stunted phenotype is due to shorter internodes, not because of an altered number of internodes (data not shown).

NbIRX8, *NbIRX9*, and *NbIRX14* are three orthologs of *Arabidopsis IRX8* (AT5G54690), *IRX9* (AT2G37090), and *IRX14* (AT4G36890) that have distinct roles in *Arabidopsis* xylan synthesis (Brown et al., 2007). All *Arabidopsis* xylan deposition-defective mutants exhibit arrested growth to some extent (Brown et al., 2007). Similarly, we observed that both VIGS-*NbIRX9* and VIGS-*NbIRX14*-infected plants exhibited curled leaves (Figure 3A, middle panel) in addition to short stature (Figure 3B, middle panel). However, less phenotypic differences were observed at the whole plant or leaf level in VIGS-*NbIRX8*-infected plants (Figure 3A and 3B, panel 2).

Phenylproponoid pathway enzymes, Caffeic acid O-methyltransferase (COMT), Cinnamoyl-CoA reductase (CCR), and 4-(hydroxy) Cinnamoyl CoA ligase (4CL), catalyze three different steps in the lignin precursor synthesis pathway (Boerjan et al., 2003). The plant morphologies resulting from silencing each of the three lignin precursor synthesis genes were strikingly different at the whole plant level (Figures 3A and 3B, right panel). VIGS-*NbCCR* and VIGS-*Nb4CL*-infected plants were much more developmentally stunted (small plants with short, thin stems and narrow, curled leaves) than the VIGS-*NbCOMT* and control plants (Figure 3A and 3B, panel 3). Eventually, the tops of VIGS-*NbCCR* and VIGS-*Nb4CL*-infected plants turned yellow and died around 10 weeks post infiltration (data not shown). In contrast, the phenotypic appearance of VIGS-*NbCOMT*-infected plants was comparable to control

Downloaded from mplant.oxfordjournals.org at Oak Ridge National Lab/UT-Battelle on September 14, 2011

plants with only slight differences in morphology (Figure 3A and 3B, right panel). Although we observed phenotypic differences in these three different categories of target genes, our semi-quantitative RT–PCR analysis suggested that TRV-based VIGS efficiently and specifically down-regulated target gene expression (Figure 3C–3E).

VIGS Plants Show Altered Cellulose, Xylan, and Lignin Deposition

To examine whether VIGS plants targeted for silencing orthologous cellulose synthesis genes from tobacco have similar or distinct cell wall polymer deposition defects and altered cell morphology similar to their respective *Arabidopsis* mutants,

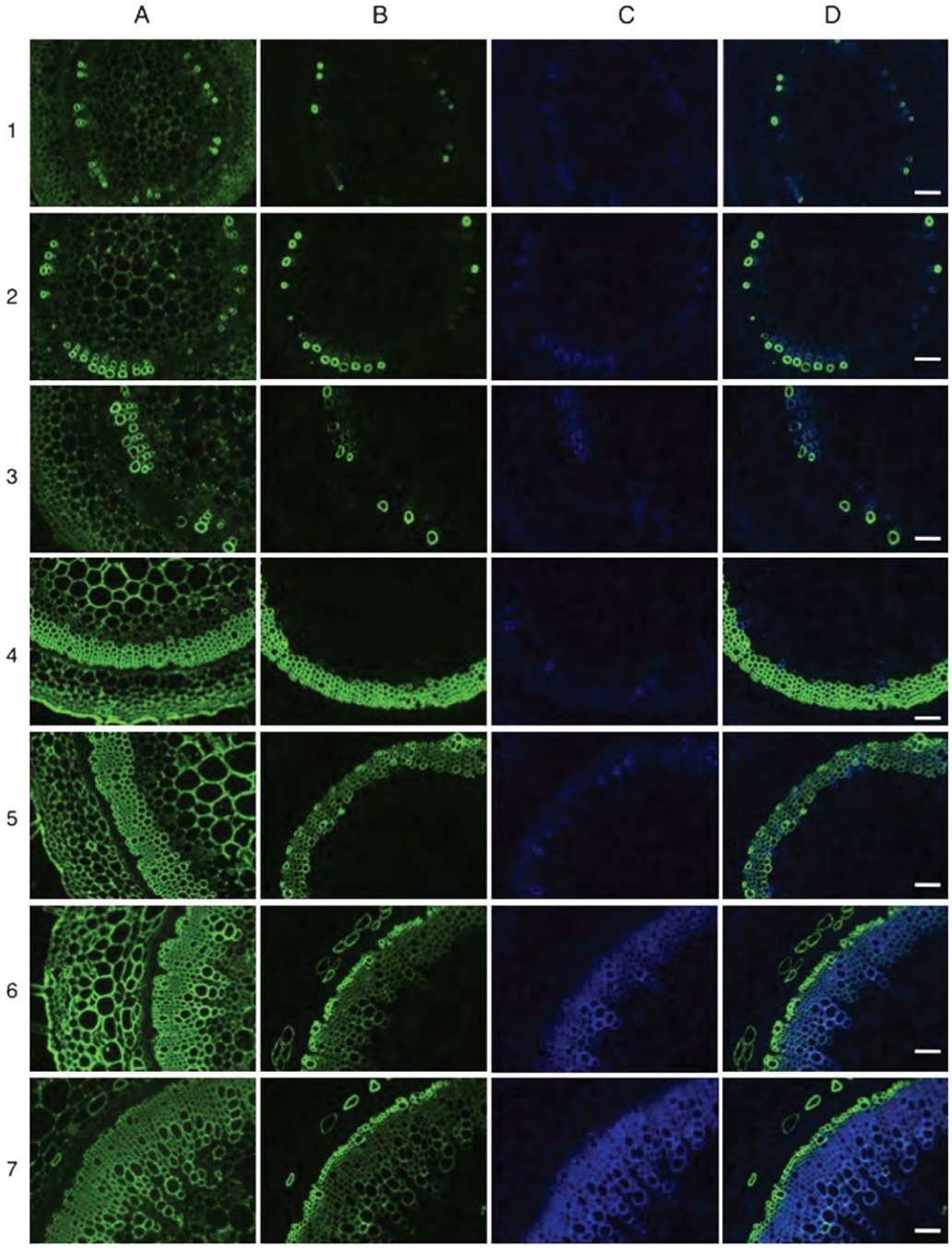

Figure 2. Cellulose, Xylan, and Lignin Deposition in VIGS Vector-Infected *N. benthamiana* Plants.

Transverse sections (TS) of the first to seventh internodes (from top to bottom as indicated on the left) of 3-wpi VIGS plants are labeled with CBM3a **(A)** and LM10 **(B)**. Green FITC signals indicate deposition of crystalline cellulose (A) and xylan (B) in respective cells. Blue autofluorescence signals from UV-illuminated TS indicate lignin deposition **(C)**. The LM10-labeled images were merged with UV-induced autofluorescence images to indicate spatial distribution of xylan and lignin in the same section **(D)**. Scale bar represents 100 μm.

Downloaded from mplant.oxfordjournals.org at Oak Ridge National Lab/UT-Battelle on September 14, 2011

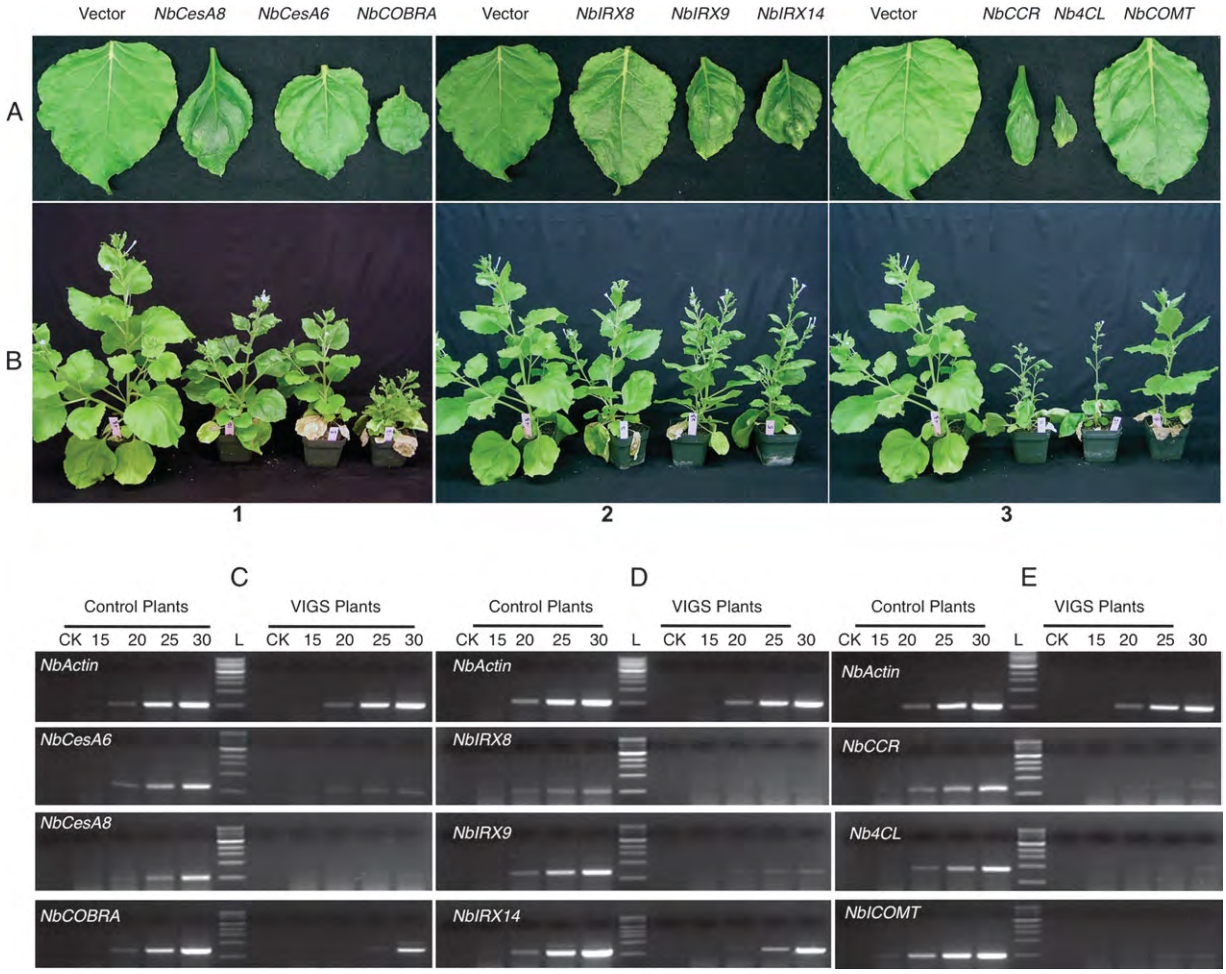

Figure 3. Morphological Phenotypes of VIGS-Mediated Silencing of Genes Involved in Cellulose, Xylan, and Lignin Synthesis and Deposition. Morphology of the fourth leaf from the top **(A)** and whole plants **(B)** of VIGS-*NbCesA8*, *NbCesA6*, and *NbCOBRA* plants (panel 1), VIGS-*NbIRX8*, *NbIRX9*, and *NbIRX14* (panel 2), VIGS-*NbCCR*, *Nb4CL*, and *NbCOMT* (panel 3) at 3 wpi is compared to that of VIGS vector-infected control plants in each panel. RT–PCR analysis indicates the reduction in the transcript levels of *NbCesA8*, *NbCesA6*, and *NbCOBRA* **(C)**, *NbIRX8*, *NbIRX9*, and *NbIRX14* **(D)**, *NbCCR*, *Nb4CL*, and *NbCOMT* **(E)** in VIGS plants. Numbers are the cycles of PCR. CK is the negative control of RT. L is the DNA ladder.

we examined TBO (toluidine blue O)-stained and CBM-labeled TS of the seventh internodes of 3-wpi VIGS plants (Figure 4A and 4B) and 14th internodes of 6-wpi VIGS plants (Figure 4C and 4D). Abnormally expanded cells were observed in the epidermis and cortex of 3-wpi VIGS-*NbCesA6* and VIGS-*NbCOBRA* infected plants seemingly due to the loss of anisotropic growth (Figure 4A, panels 2 and 3). The secondary xylem of 3 and 6-wpi VIGS-*NbCesA6* plants had the same organization and cell structure as that of the control plants (Figure 4A and 4C, panels 1 and 2). In comparison, VIGS-*NbCOBRA*-infected plants had misarranged and smaller secondary xylem vessels, in addition to strikingly bulgy and malformed cortex cells (Figure 4A, panel 3). Radially elongated cells were also observed in the secondary xylem of 6-wpi VIGS-*NbCOBRA*-infected plants (Figure 4C, panel 3), which is likely due to uncontrolled anisotropic expansion as previously reported in elongating root cells (Baskin, 2005; Roudier et al., 2005). By contrast, VIGS-*NbCesA8*-infected plants showed normal epidermis and cortex cells, but collapsed and irregular xylem in young and old stems (indicated by arrows in Figure 4A and 4C, panel 4). Additionally, CBM3a labeling indicated that less crystalline cellulose deposition occurred in the cortex, but it remained essentially unchanged in xylem tissues of both VIGS-*NbCesA6* and VIGS-*NbCOBRA*-infected plants compared to control and VIGS-*NbCesA8*-infected plants (Figure 4B and 4D, panels 2–4). By contrast, crystalline cellulose deposition was significantly reduced in secondary xylem tissues of VIGS-*NbCesA8*-infected plants, and largely remained unchanged in the cortex compared to control, VIGS-*NbCesA6*, and VIGS-*NbCOBRA* plants (Figure 4B and 4D, panel 4). Interestingly, reduction of cellulose in the secondary xylem tissue of 6-wpi VIGS-*NbCesA8*-infected plants is reflected by an uneven cellulose deposition pattern (Figure 4D, panel 4), which was not

Downloaded from mplant.oxfordjournals.org at Oak Ridge National Lab/UT-Battelle on September 14, 2011

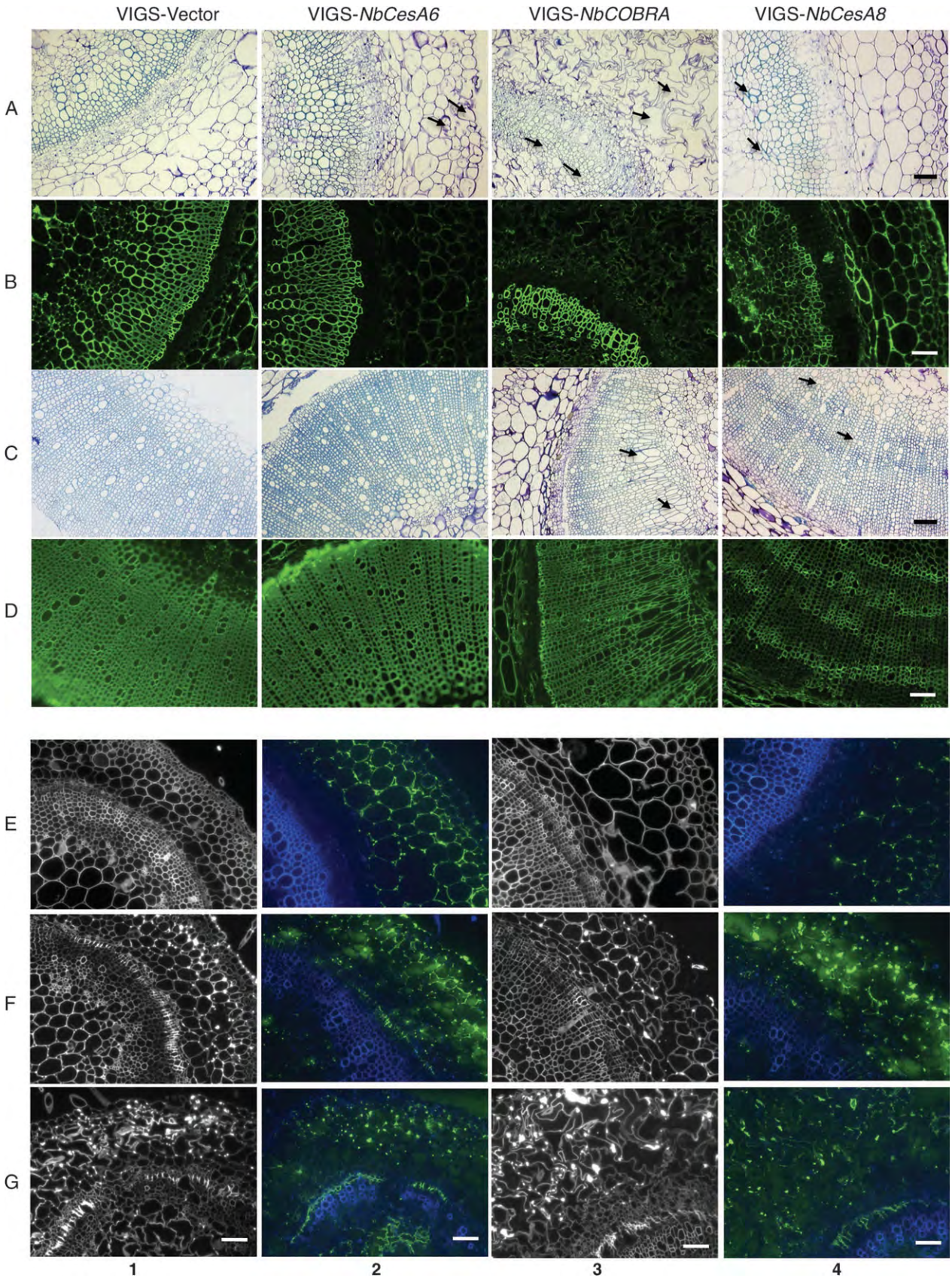

Figure 4. Alteration of Anatomical Structures and Cellulose and Xyloglucan Deposition in VIGS Plants.

Downloaded from mplant.oxfordjournals.org at Oak Ridge National Lab/UT-Battelle on September 14, 2011

detected in control, VIGS-*NbCesA6*, and VIGS-*NbCOBRA*-infected plants (Figure 4D, panels 1–3).

Similar cellulose deposition defects in the primary cell wall of *NbCesA6* and *NbCOBRA*-silenced plants prompted us to examine whether *NbCOBRA* has a role similar to *NbCesA6* in primary cell wall formation. We stained TS of the fifth and seventh internodes with Calcofluor White (CW), which is used to detect cellulose and other glucans (e.g. callose) (Wood et al., 1983). We observed bright CW-stained speckles in the cortex and a bright band of several layers of stained cells in the cambial zone of both VIGS-*NbCesA6* (Figure 4F, panels 1 and 3) and VIGS-*NbCOBRA* plants (Figure 4G, panels 1 and 3), but not in the control plants (Figure 4E, panels 1 and 3). To determine whether this abnormal deposition consists of callose, as was the case in the *Arabidopsis Atcob-5* mutant (AT5G60920) (Ko et al., 2006), we stained TS of the same internodes using Aniline Blue Fluorochrome, which specifically detects callose (Stone et al., 1984). However, the staining pattern was dissimilar to that of CW staining (data not shown), suggesting these abnormal deposits may not be composed of callose. To determine whether the CW-stained polymer is actually xyloglucan, we probed TS with the anti-xyloglucan antibody, LM15, which binds strongly to non-fucosylated xyloglucan in tobacco stem sections (Marcus et al., 2008). We observed bright LM15-labeled xyloglucan aggregated in intercellular spaces in the cortex of VIGS-*NbCesA6* and VIGS-*NbCOBRA* plants (Figure 4F and 4G, panels 2 and 4), but not in the control plants, where xyloglucan is deposited at the junctions between adhered and non-adhered cell walls at intercellular spaces (Figure 4E, panels 2 and 4). Furthermore, similar to the CW staining patterns, LM15-labeled cells formed a bright band in the cambial region of young internodes of both VIGS-*NbCesA6* and VIGS-*NbCOBRA* plants, but not in the control plants (Figures 4F and 4G, panels 2 and 4). Collectively, our results suggest that *NbCOBRA* has a role in cellulose deposition similar to *NbCesA6*. Down-regulating *NbCOBRA* and *NbCesA6* might be interrupting cellulose and xyloglucan interactions, leading to deposition of disorganized xyloglucan that is stained by CW and the LM-15 antibody.

Our studies of the secondary xylem using TBO-stained 3 and 6-wpi VIGS plants showed less organized xylem tissues and prominent irregular xylem vessels in TS of the seventh and 14th internodes of VIGS-*NbIRX9* and *NbIRX14* (Figure 5A and 5C, panels 3 and 4), but less apparent irregular xylem cells in TS of the seventh and 14th internodes of VIGS-*NbIRX8* plants (Figure 5A and 5C, panel 2). The deposition of xylan, as determined by LM10 immunolabeling of TS of the seventh and 14th internodes, revealed strong fluorescence signals in developing xylem tissues of the control plants, especially in several layers of unlignified cells near the cambial zone. In contrast, weak, non-contiguous fluorescence signals were observed in VIGS-*NbIRX8*, VIGS-*NbIRX9*, and VIGS-*NbIRX14* plants (Figure 5B and 5D, panels 2–4), which indicates that down-regulating *NbIRX8*, *NbIRX9*, and *NbIRX14* all reduced LM10-recognized xylan content. Our results suggest that VIGS mediates an efficient silencing of genes in the xylan synthesis pathway and that *NbIRX8*, *9*, and *14* genes function similarly to their *Arabidopsis* orthologs.

To examine the xylem phenotypes of VIGS-*NbCOMT*, Nb*CCR*, and *Nb4CL* in *N. benthamiana* plants, we compared the structure of vascular tissues of TBO-stained TS (Figure 6A and 6C). We observed a large proportion of collapsed xylem elements that appeared early on in the seventh internodes of 3-wpi VIGS-*NbCCR* and VIGS-*Nb4CL* plants (Figure 6A, panels 3 and 4). This phenomenon became more pronounced in the 14th internodes of 6-wpi VIGS plants (Figure 6C, panels 3 and 4). By contrast, xylem tissues of the seventh and 14th internodes of VIGS-*NbCOMT*-infected plants showed no such dramatic morphological changes compared to the control plants (Figure 6A and 6C, panel 2), except for a slight difference in the organization of xylem elements at early stages as shown in the seventh internode (Figure 6A, panel 2), in which disconnected xylem elements were observed. Based on the UV-induced autofluorescence assay, much less lignin deposition in secondary xylem tissue occurred early in the seventh internodes in which overall autofluorescent signals were much weaker in VIGS-*NbCCR* and VIGS-*Nb4CL*-infected plants than in the control plants (Figure 6B, panels 3 and 4). Interestingly, no lignin autofluorescence signals were observed in the 14th internodes of both VIGS-*NbCCR* and VIGS-*Nb4CL*-infected plants (Figure 6D, panels 3 and 4). We observed that the autofluoresence signals from TS of the seventh internode of VIGS-*NbCOMT* were comparable to those of the control plants (Figure 6B, panel 2). However, autofluorescence signals in the TS of 14th internode of VIGS-*NbCOMT*-infected plants were unevenly distributed (Figure 6D, panel 2), slightly contrasting with the uneven fluorescent signals we observed in VIGS-*NbCesA8* and VIGS-*NbIRX*s-infected plants. These results indicate that VIGS is also an effective approach for targeting genes in the lignin synthesis pathway.

Irregular cortex cells of VIGS-*NbCesA6* (2) and VIGS-*NbCOBRA* plants (3) and irregular xylem cells of VIGS-*NbCesA8* (4) and VIGS-*NbCOBRA* plants (3) are indicated with arrows in TBO-stained TS of seventh internodes **(A)** and 14th internodes **(C)**. Reduced crystalline cellulose deposition in the cortex of VIGS-*NbCesA6* (2) and VIGS-*NbCOBRA* plants (3), and xylem cells of VIGS-*NbCesA8* plants (4) is indicated by weak, uneven green FITC-signals compared to the control plants in CBM3a-labeled TS of seventh internodes **(B)** and 14th internodes **(D)**. Bright speckles in UV-illuminated Calcofluor-White-stained TS indicate abnormal deposition in the fifth internode (1) and seventh internode (3) of VIGS-*NbCesA6* **(F)** and VIGS-*NbCOBRA* **(G)** plants compared to control plants **(E)**. Bright FITC fluorescent bands and aggregated spots in LM15-immunolabeled TS of fifth internode (2) and seventh internode (4) indicate an abnormal xyloglucan deposition in cambium and cortex of VIGS-*NbCesA6* (F) and VIGS-*NbCOBRA* plants (G). Pictures are FITC and UV merged images and blue fluorescence signals are UV-induced lignin autofluorescence, indicating secondary xylem cells. Scale bar represents 100 μm.

Downloaded from mplant.oxfordjournals.org at Oak Ridge National Lab/UT-Battelle on September 14, 2011

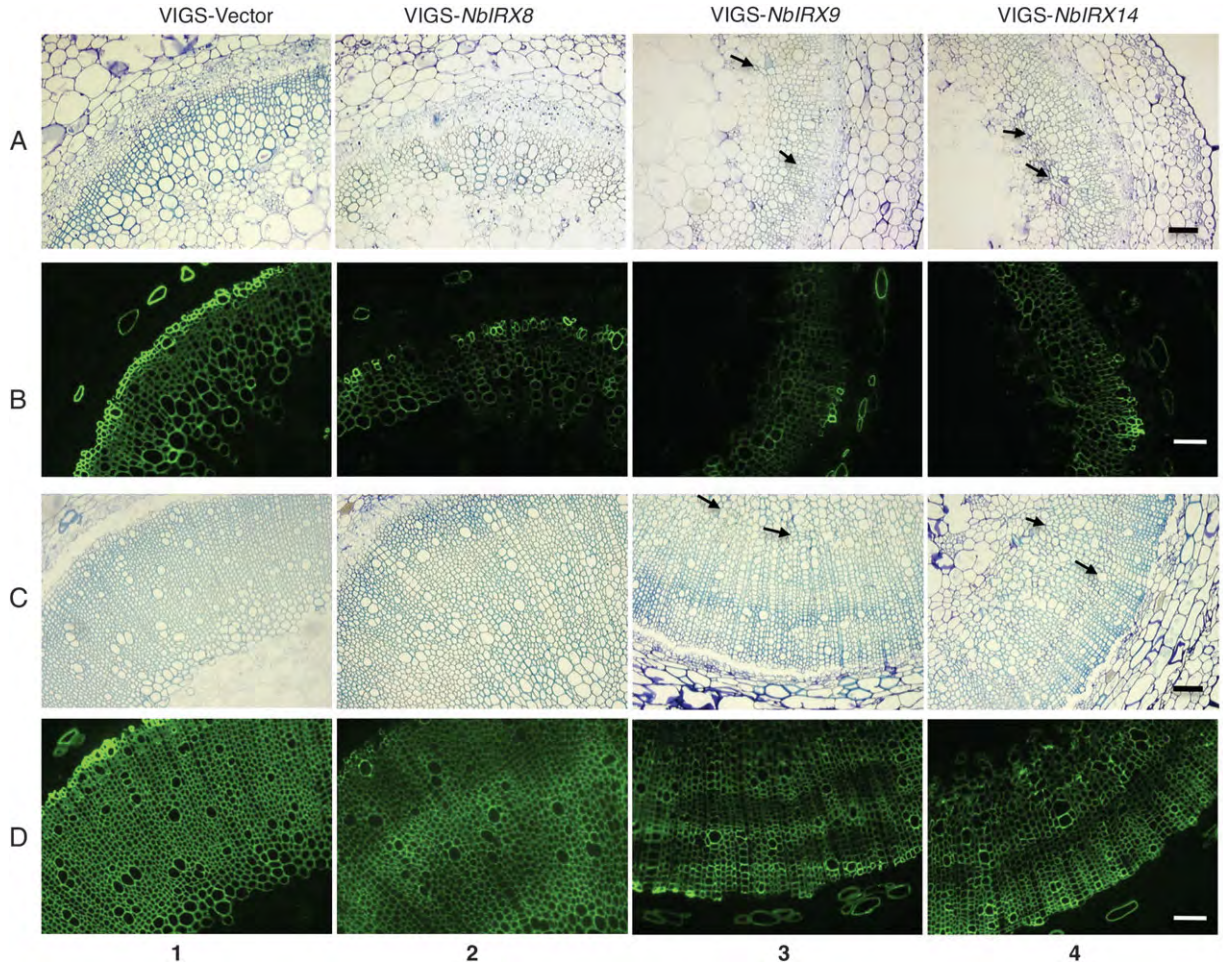

Figure 5. Alteration of Anatomical Structures and Xylan Deposition in VIGS Plants.

Irregular xylem cells are indicated with arrows in TBO-stained TS of seventh internode **(A)** and 14th internodes **(C)** of *NbIRX9* (3) and VIGS-*NbIRX14* plants (4). A reduction in xylan deposition in xylem cells of VIGS-*NbIRX8* (2), *NbIRX9* (3), and VIGS-*NbIRX14* (4) plants is indicated by the weak, uneven green FITC-signals compared to the control plants in LM10-immunolabeled TS of seventh internodes **(B)** and 14th internodes **(D)**. Scale bar represents 100 μm.

Determination of Crystalline Cellulose and Xylan Contents in VIGS Plants Using CoMPP

Previously, the comprehensive microarray polymer profiling (CoMPP) technique has been successfully used for systematic mapping of cell wall glycans in a semi-quantitative high-throughput fashion (Moller et al., 2007). To confirm our results of CBM3a and LM10-mediated labeling of plant tissue sections and also to investigate whether CoMPP can be used as a downstream detection assay to aid in screening candidate genes involved in cellulose and xylan biosynthesis, we applied CoMPP for the detection of cellulose and xylan using our VIGS plants.

Stem extracts from VIGS plants were arrayed on the nitrocellulose membranes manually. The membranes were probed with CBM3a and LM10 for determining crystalline cellulose and xylan content, respectively. As indicated in Figure 7, microcrystalline cellulose and xylans were detected on the array in amounts as low as 8 ng. A major reduction of crystalline cellulose in the stems of VIGS-*NbCesA8* but not in the stems of VIGS-NbCesA6, VIGS-*NbCOBRA*, and VIGS-*NbIRX8* was observed (Figure 7A). Similarly, a significant reduction of LM10 recognized xylan in the stems of VIGS-*NbIRX8*, VIGS-*NbIRX9*, and VIGS-*IRX14*-infected plants was clearly observed on the xylan array (Figure 7B) compared to that of the control plants. Xylan content of VIGS-*NbCesA8*-infected plants was comparable to that of the control plants. These results suggest that the modified CoMPP technique is sufficiently sensitive for determination of alteration of cellulose and xylan contents resulting from VIGS of corresponding genes and therefore it could be employed in a high-throughput screen for novel cell wall genes.

Determination of Extractability of VIGS Plants Using Cell Wall Glycan-Directed Monoclonal Antibody ELISA

We hypothesized that reducing cellulose, xylan, lignin, or any other wall components will alter the overall structure of the cell wall, which, in turn, might affect cell wall extraction

Downloaded from mplant.oxfordjournals.org at Oak Ridge National Lab/UT-Battelle on September 14, 2011

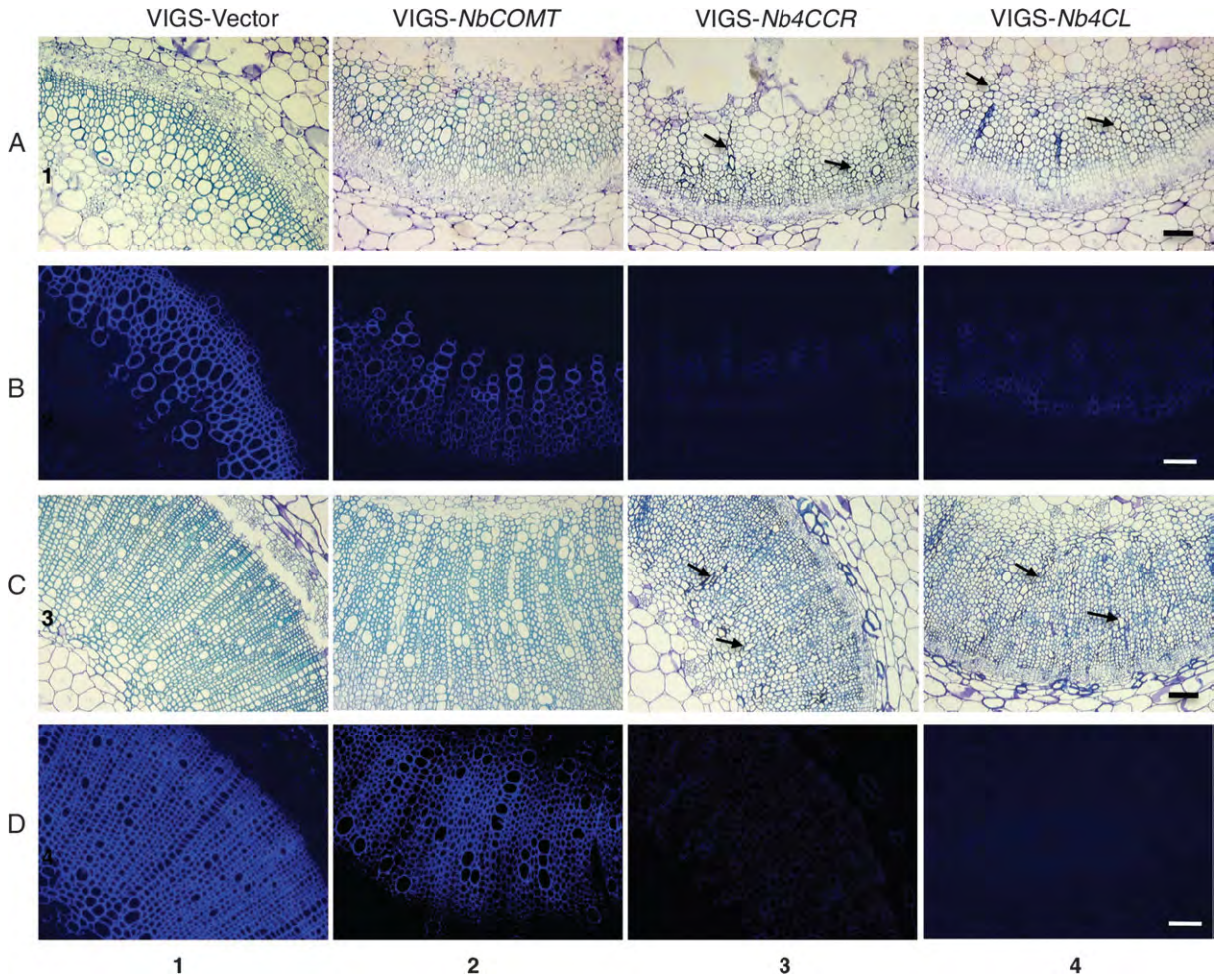

Figure 6. Alteration of Anatomical Structures and Lignin Deposition in VIGS Plants.

Irregular xylem cells are indicated by arrows in TBO-stained sections of seventh internodes **(A)** and 14th internodes **(C)** of *NbCCR* (3) and VIGS-*Nb4CL* plants (4). Differences in lignin deposition in secondary xylem cells of VIGS-*NbCOMT* (2), *NbCCR* (3), *Nb4CL* (4), and the control plants (1) are indicated by the intensity of blue autofluorescence signals in UV-illuminated TS of seventh internodes **(B)** and 14th internodes **(D)**. Scale bar represents 100 μm.

properties. To test this hypothesis and also to test whether VIGS can be used for screening or evaluating functions of genes that affect cell wall extractability, we adapted a cell wall glycan-directed monoclonal antibody-ELISA (Pattathil et al., 2010) for detecting cell wall glycome-profiling patterns from sequentially extracted cell wall fractions of VIGS plants in which cellulose, xylan, and lignin were reduced. We collected woody stems of 10-wpi VIGS-*NbCesA6*, VIGS-*NbCesA8*, VIGS-*NbIRX8*, VIGS-*NbIRX9*, VIGS-*NbIRX14*, and VIGS-*NbCOMT* plants and prepared cell walls from them. VIGS-*NbCOBRA*, VIGS-*Nb4CL*, and VIGS-*NbCCR* plants were not examined because we were unable to collect enough stem material due to severe growth defects in these VIGS plants. We sequentially extracted cell wall polymers from the stem cell walls and probed the polymers released in each extract using 150 cell wall carbohydrate-directed monoclonal antibodies (Pattathil et al., 2010) to yield glycome profile patterns for each extract. These 150 antibodies fall into 18 groups that recognize epitopes present on most major classes of polysaccharides present in plant cell walls, including non-fucosylated (NON-FUC) and fucosylated (FUC) xyloglucans (XGs), various types of xylans (Xylan 1–4), pectins, and arabinogalacatans (Pattathil et al., 2010). Differences in the glycome profile patterns of VIGS plants from those of controls reflect alterations in the extractability of cell wall polymers. As shown in Figure 8, glycome profiles of VIGS-*NbCesA8* and VIGS-*NbCOMT* plants are strikingly different in comparison to the control and other VIGS plants. For VIGS-*NbCesA8* plants, the most dramatic differences appeared in non-fucosylated xyloglucan, xylan-3, and xylan-4 profiles. In contrast to the control plants, more non-fucosylated xyloglucan, xylan-3, and xylan-4 epitopes were detected in the 1 M KOH fraction, but much less or none in the 4 M KOH. In addition, the level of xylan-3 and xylan-4 epitopes was also higher in the chlorite fraction of

Downloaded from mplant.oxfordjournals.org at Oak Ridge National Lab/UT-Battelle on September 14, 2011

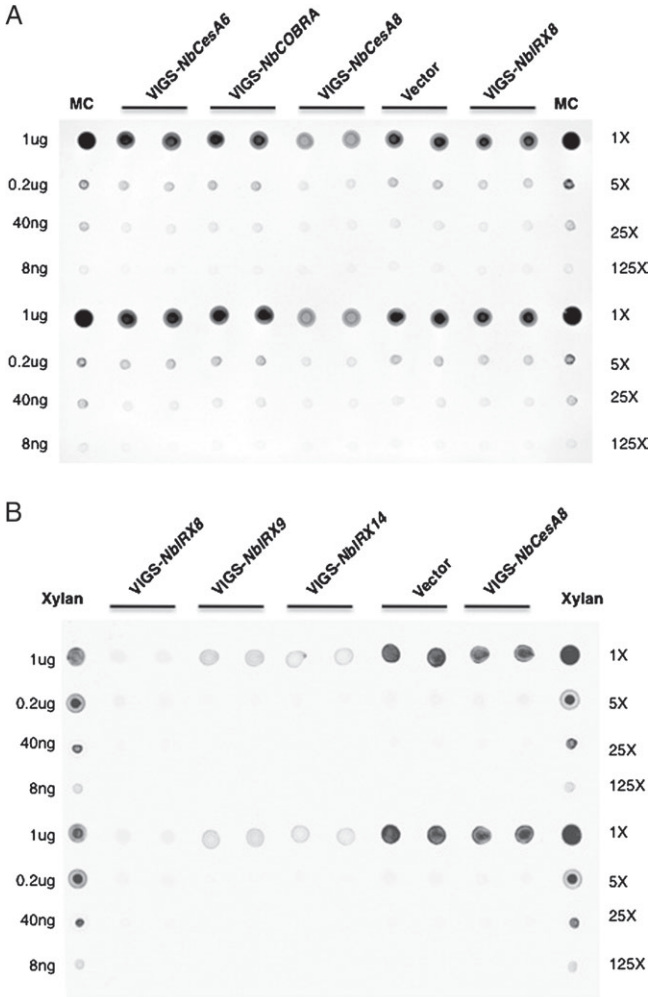

Figure 7. CoMPP Analysis of Crystalline Cellulose and Xylan.

Crystalline cellulose **(A)** and xylan **(B)** CoMPP analysis of VIGS plant stems. Two microliters of serial dilution of Cadoxen extracts (A) and NaOH extracts (B) of VIGS plant stems were printed in quadruplicate onto a nitrocellulose membrane. Each sample is represented on the array by 16 spots. Positions of commercial microcrystalline cellulose (MC), birchwood xylan, and extracts of VIGS plants are indicated on the top of each array. Amounts of microcrystalline cellulose and xylan are indicated on the left of the array; dilution factors of extract are indicated on the right of the array.

VIGS-*NbCesA8* plants than in that of the control plants. For VIGS-*NbCOMT* plants, high levels of xylan-3 and xylan-4 and RG-1/arabinogalactan and arabinogalactan epitopes (RG-1/AG and AG-4) were detected in the ammonium oxalate fraction, a mildly extracted fraction, and dramatically reduced levels of diverse RG-1/arabinogalacatan, pectic backbone, and arabinogalactan epitopes (RG-1/AG, pectic backbone and AG-1 through 4) were detected in the 4 M KOH fraction compared to the control plants. In contrast, VIGS-*NbIRX8*, VIGS-*NbIRX9*, and VIGS-*NbIRX14* plants have similar glycome profiles, which are, however, still different from the profiles of control plants. Much lower levels of xylan-3 and xylan-4 epitopes were detected in the carbonate fraction and higher levels of non-fucosylated xyloglucan epitopes in the 1 M KOH fraction of VIGS-*NbIRX8*, VIGS-*NbIRX9*, and VIGS-*NbIRX14* plants than in the profiles of control plants. VIGS-Nb*CesA6* plants showed some differences in glycome profiles compared to the control plants. However, overall, a lower level of antibody binding was detected in the extracts from VIGS-*NbCesA6* plants compared to those of control plants, which may be due to some extent to the growth defects in VIGS-*NbCesA6* plants. In summary, the glycome profiles suggest that reduction of cellulose or lignin dramatically changes the overall structure of the cell wall and thus has profound effects in the cell wall extractability, whereas reduction of xylan has a less profound effect on cell wall structure and extractability.

DISCUSSION

Here, we demonstrate that TRV-based VIGS in *N. benthamiana* is an effective approach for studying cell wall biology. Our results show that *N. benthamiana* stems possess characteristics

Downloaded from mplant.oxfordjournals.org at Oak Ridge National Lab/UT-Battelle on September 14, 2011

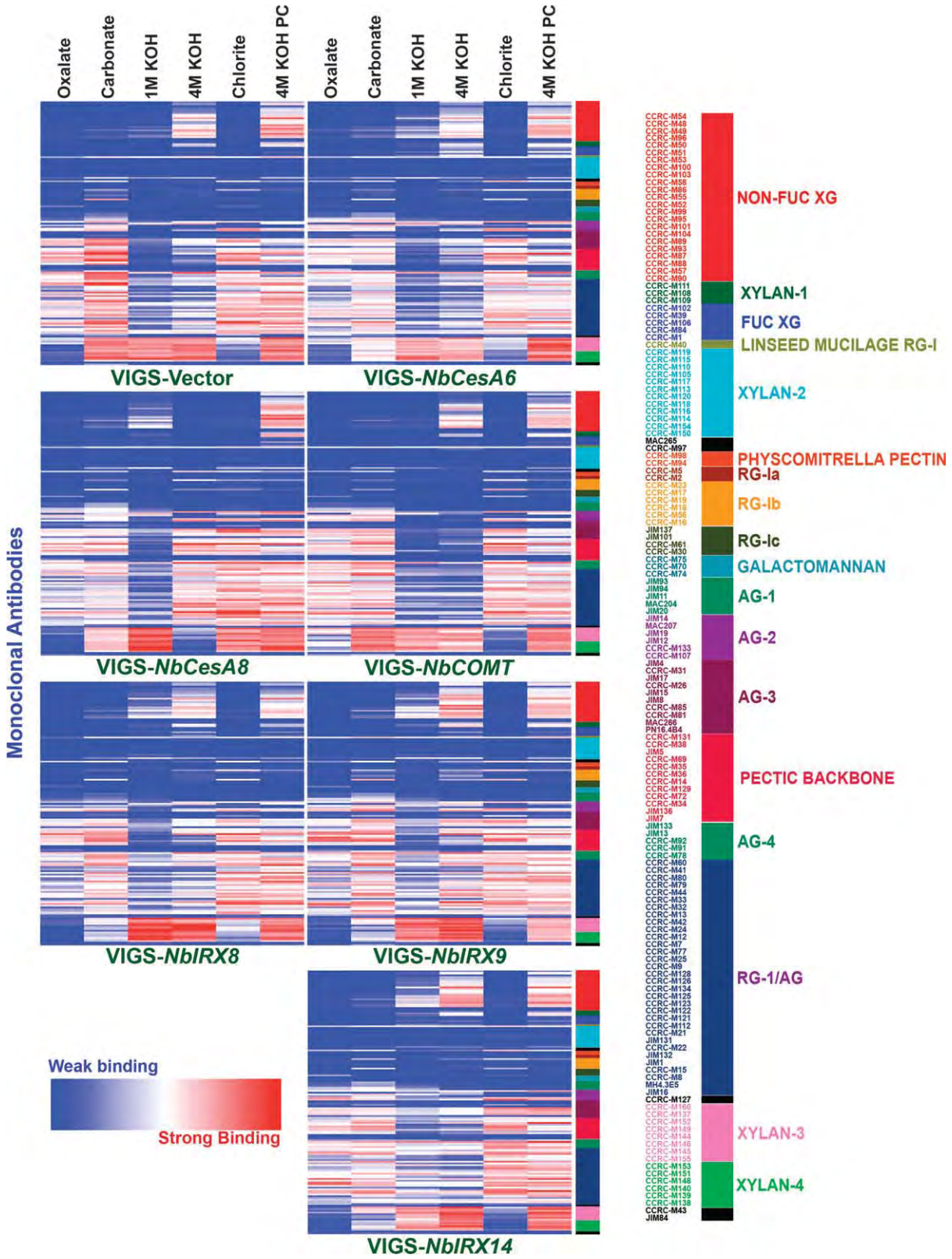

Figure 8. Glycome Profiling of Sequential Stem Wall Extracts of VIGS Plants.

Downloaded from mplant.oxfordjournals.org at Oak Ridge National Lab/UT-Battelle on September 14, 2011

of primary and secondary cell wall structure and composition that are similar to those of woody plants, such as poplar, that undergo prolonged secondary growth. TRV-based VIGS can efficiently down-regulate target genes associated with both primary and secondary cell wall formation in the stems. Our results also show that VIGS-mediated silencing of genes involved in cellulose, xylan, and lignin synthesis produces distinct phenotypes, which are similar to those revealed by using other gene silencing systems in other plants. The specificity of TRV-based VIGS is highlighted by the contrasting effects of silencing of different *CesA* genes on plant morphology, cell structure, and cell wall composition. Silencing of *NbCesA6* was associated with alterations in cell wall structure and cellulose deposition in primary cell walls. By contrast, silencing of *NbCesA8* caused collapsed xylem cells and a greater reduction of cellulose deposition in secondary cell walls, with fewer effects on primary cell wall structure and composition. Our results clearly suggest that TRV-based VIGS provides a novel system for simultaneous and rapid comparison of the functions of various genes related to cell wall formation. In addition to these 'proof of concept' results, our data also support conservation of functions of targeted genes in cell wall formation among different species. Furthermore, our results provide new insights into how these cell wall-related genes affect secondary growth originating from the vascular cambium of woody stems and how structural alteration of secondary growth-derived tissues affect cell wall biomass extractability. Although the functions of most of the genes targeted by VIGS in this study have been characterized in other plants, we report new insights into their functions in establishing normal structures during secondary growth, especially in the case of *NbCOBRA* and *NbIRX* genes, which have not been reported in *N. benthamina* plants or other plant species.

Mosaic CBM3a and LM10-labeling patterns and uneven UV-induced autofluorescence distributions in VIGS plants indicate partial reduction of cellulose, xylan, and lignin presumably as a result of partial silencing of target genes by VIGS (Figures 4, 5, and 6D). This typical uneven pattern may be due to the transient nature of VIGS resulting in temporal and spatial differences in the silencing efficiency of the targeted genes. Cell wall macromolecule deposition patterns may also be relevant to the patterns of virus infection, as described in an earlier study (Burton et al., 2000). However, this may not be the case, since the uneven localization patterns appear to be different among the different VIGS plants. Moreover, in VIGS-*NbCCR* and VIGS-*Nb4CL* plants, we observed relatively even lignin reduction in the stem. Furthermore, a similar uneven gene silencing effect was observed in stable transgenic plants, in which a 'patchy' distribution of down-regulated 4CL proteins was visualized by immunolocalization in stem cross-sections (Kajita et al., 1997). Taken together, these results suggest that uneven patterns that reflect partial loss of function of genes may be the nature of RNAi, not specific to VIGS.

The synthesis of xylan, a major constituent of hemicellulose, particularly in secondary walls, is not fully understood (York and O'Neill, 2008). Previous studies suggested that IRX9 and IRX14 are required to synthesize the backbone of xylan, whereas IRX8 may be involved in the synthesis of a xylan primer (Brown et al., 2007; Peña et al., 2007). It is undetermined whether *NbIRX8*, *NbIRX9*, and *NbIRX14* have the same roles as *AtIRX8*, *AtIRX9*, and *AtIRX14* in xylan synthesis in *N. benthamiana*. However, we clearly show that down-regulation of *NbIRX8*, *NbIRX9*, or *NbIRX14* by VIGS causes a dramatic reduction in LM10-recognized xylan epitopes. The more severe morphological, structural, and xylan-defective phenotypes of VIGS-*NbIRX9* and *NbIRX14* appear to have similar roles in xylan synthesis in *N. benthamiana* plants as in *Arabidopsis*. In contrast, VIGS-*NbIRX8* plants showed less xylan content in the CoMPP arrays and slightly different intensity distribution of uneven LM10 labeling patterns, with less severe morphological and structural phenotypes. In addition, the profiling patterns using xylan-directed antibodies in wall extracts from VIGS-*NbIRX9* and VIGS-*NbIRX14* are much more similar to each other than to the profiles of VIGS-*NbIRX8* wall extracts (Figure 8). This suggests that NbIRX8 may have a distinct role from VIGS-*NbIRX9* and VIGS- *NbIRX14* in xylan synthesis. Although cell wall glycan profiling does not quantitatively indicate differences in cell wall polymer contents, we noticed that the epitopes recognized by the xylan-3 and xylan-4 antibodies were not significantly reduced in VIGS-*NbIRX8*, VIGS-*NbIRX9*, and VIGS-*NbIRX14* plants compared to the control plants. Therefore, down-regulation of *NbIRX8*, *NbIRX9*, and *NbIRX14* most likely leads to a significant reduction in some forms of xylan, but may have less of an effect on other xylan epitopes, although this needs verification through detailed compositional and structural studies of the xylans in these plants.

A tobacco model system was used previously to understand lignin biosynthesis (Anterola and Lewis, 2002). We found that the phenotypes of VIGS-*NbCOMT*, VIGS-*NbCCR*, and VIGS-*Nb4CL*-infected plants were strikingly similar to those of stable transgenic tobacco plants (Anterola and Lewis, 2002). For

Sequential stem cell wall extracts of 10-wpi VIGS-*NbCesA6*, VIGS-*NbCesA8*, VIGS-*NbCOMT*, VIGS-*NbIRX8*, VIGS-*NbIRX9*, VIGS-*NbIRX14*, and VIGS-vector control plants were generated as described in Methods. The presence of cell wall glycan epitopes in each extraction fraction was determined by ELISAs using 150 glycan-directed monoclonal antibodies (Pattathil et al., 2010) and the data presented as heat maps. Reagents used for extracting stem materials are indicated on the top of each column. The panel on the right lists the array of antibodies used (left-hand side) grouped according to the principal cell wall glycan (right-hand side) recognized by the antibodies. The blue-white-red scale indicates the strength of the ELISA signal: bright red, white, and dark blue colors depict strongest binding, medium binding, and no binding, respectively.

Downloaded from mplant.oxfordjournals.org at Oak Ridge National Lab/UT-Battelle on September 14, 2011

example, similar to our VIGS-*NbCCR*-infected plants, *CCR*-down-regulated transgenic tobacco was severely stunted with spoon-like leaves. We also observed collapsed xylem vessels, again similar to those found in *CCR*-down-regulated transgenic tobacco plants (Piquemal et al., 1998; Chabannes et al., 2001). *4CL*-down-regulated transgenic tobacco plants had unusual brownish-green stems and severe dwarfing (Atanassova et al., 1995; Zhong et al., 1998), similar to our VIGS-*Nb4CL*-infected plants. Contradictory observations of the effects of *COMT* down-regulation have been reported previously (Anterola and Lewis, 2002). Collectively, *COMT* suppression apparently has a fairly moderate or no effect on overall lignin content in tobacco, with only one exception (Ni et al., 1994). Based on the phenotypes and the degree of reduced *NbCOMT* mRNA levels in VIGS-*NbCOMT*-infected plants, we conclude that down-regulation of *NbCOMT* has only moderate effects on lignin deposition, evidenced by less severe morphological phenotypes, almost unaltered secondary xylem structure, and less lignin reduction in these plants. Nonetheless, the glycome profiles of cell wall extracts from VIGS-*NbCOMT* plants were different from control plants. This indicates that a moderate reduction of lignin in *N. benthamiana* plants does not significantly alter plant growth, but can have profound effects on cell wall extractability.

Functional roles for *COBRA* genes in cell wall formation and cell expansion have been identified in *Arabidopsis*, rice, and maize systems (Schindelman et al., 2001; Li et al., 2003; Brown et al., 2005; Persson et al., 2005; Roudier et al., 2005; Ching et al., 2006). Here, our data provided some new insights into the function of *COBRA* in stem development. Based on sequence analysis, *NbCOBRA* shares 72 and 70% identity with *AtCOBRA* (AT5G60920) and *AtCOBL4* (AT5G15630), respectively. The severely dwarfed phenotypes of VIGS-*NbCOBRA* are very similar to those of the *Arabidopsis cobra* mutant (Roudier et al., 2005), but are unlike the phenotypes of the *Atcobl4* mutant (Brown et al., 2005), indicating that VIGS most likely targeted the *N. benthamiana* counterpart of *AtCOBRA*. Since the *Arabidopsis cobra* mutant is severely stunted and has no inflorescence stem development, most of the loss-of-function morphological and structural phenotypes were characterized in the roots of this mutant, but not in the aerial parts (Roudier et al., 2005). Here, we clearly show that silencing of *NbCOBRA* affects cell anisotropic expansion in stems, which leads to the alteration of both primary and secondary wall structures of the stem tissues. Bulging root morphology resulting from uncontrolled radial growth of cortex and epidermal cells in the root elongation zone was replicated in the stem cortex and pith of VIGS-*NbCOBRA* plants. Additionally, aggressive radial expansion of parenchyma cells in xylem tissues was observed in older internodes of VIGS-*NbCOBRA*-infected plants. Reduced cellulose deposition and aggregation of xyloglucan in the primary cell walls of VIGS-*NbCOBRA* plants suggests that *NbCOBRA* regulates cellulose deposition in the primary cell wall. It is undetermined whether defective cellulose deposition results from the loss of function of the *NbCOBRA* gene, as is observed in VIGS-*NbCesA6* plants. However, based on *in situ* CBM3a labeling of young and older internodes and cellulose array data, we conclude that down-regulating *NbCOBRA* has less of an effect on cellulose content in secondary xylem tissues.

The stems of 10-wpi VIGS plants appear to be ideal woody materials for determining comparatively how cell wall compositions affect the extractability of cell wall polymers. Cell wall glycome profiling of VIGS plants in this study show that reduction of cellulose and lignin can have profound effects on cell wall extractability. The fact that moderate reduction of lignin in the VIGS-*NbCOMT* plant stems results in a more facile release of xylan-3, xylan-4, and most arabinogalactan epitopes from cell wall materials suggests that such genetic manipulation may have the potential to reduce the recalcitrance of biomass. Specifically, down-regulation of *NbCOMT* has a less severe impact on growth compared to the down-regulation of other genes in the lignin biosynthetic pathway, such as *Nb4CL* and *NbCCR*. Reduction of at least some forms of xylan that resulted from the down-regulation of *NbIRX8*, *NbIRX9*, and *NbIRX14* has a mild effect on cell wall extractability. Despite the important functions of IRX8, IRX9, and IRX14 in xylan biosynthesis, the overall effects of down-regulating *IRX8*, *IRX9*, and *IRX14* on cell wall structure and extractability are similar, as exemplified by their similar glycome profiling patterns. This implies that it is possible to infer the function of targeted genes in the overall structure of cell walls based on glycome profiling patterns. From this perspective, the VIGS approach in *N. benthamiana* plants provides an ideal system for creating a glycome profiling database, from which one may gain inferences about the functions of genes in cell wall composition, structure, and extractability based on the glycome profiling patterns.

In conclusion, TRV-based VIGS exhibits a high level of reproducibility, efficiency, and specificity in silencing cell wall-related genes. Furthermore, this approach provides a fast, reliable, and robust reverse genetic platform for studying plant cell wall formation, on which plant morphology, anatomy, and cell wall composition and extractability can be simultaneously characterized in a rapid manner. Therefore, in combination with different downstream assays, like the CoMPP and cell wall glycome profiling approaches used in this study, VIGS has great potential to be adapted for high-throughput studies to identify novel genes involved in cell wall synthesis and cell wall structures. The availability of a large number of antibodies against diverse cell wall glycan epitopes (Pattathil et al., 2010) greatly facilitates the identification of genes involved in dynamic and complex biosynthetic pathways that lead to cell wall formation. A well designed, specially constructed cDNA library from specific cell types will facilitate discovery of novel enzymatic and regulatory proteins in these pathways. Transferring the knowledge acquired from this kind of functional screening in readily transformable plants to

Downloaded from mplant.oxfordjournals.org at Oak Ridge National Lab/UT-Battelle on September 14, 2011

other plant species, such as poplar trees (Joshi et al., 2004), has a potential to provide an effective strategy for increased production of improved lignocellulosic raw materials for efficient bioconversion to bioenergy.

METHODS

VIGS Constructs

cDNAs were synthesized using 2 μg of total RNA isolated from the stems of *N. benthamiana* plants and SuperScript reverse transcriptase (Invitrogen) according to the manufacturer's protocol. Primers used for amplifying *NbCesA6*, *NbCesA8*, *NbCOBRA*, *NbIRX8*, *NbIRX9*, *NbIRX14*, *NbCOMT*, *NbCCR*, and *Nb4CL* and corresponding *Arabidopsis* orthologs are listed in Supplemental Table 1. Resulting gene fragments were cloned into VIGS vector pTRV2 (Dong et al., 2007) and confirmed by DNA sequencing.

Plant Growth and Agroinfiltration

N. benthamiana plants were grown in pots at 23°C under continuous light. DNA plasmids of pTRV1, pTRV2, and pTRV2 derivatives were transformed into *Agrobacterium tumefaciens* strain GV2260 using a heat shock protocol (Dong et al., 2007). Overnight-grown *Agrobacterium* cultures were spun and cells were re-suspended in infiltration medium (10 mM MES, 10 mM $MgCl_2$, 200 μM acetosyringone). Cell suspensions were incubated at room temperature for 3 h prior to infiltration into the leaves of 3-week-old seedlings (Zhu and Dinesh-Kumar, 2008a, 2008b). VIGS experiments were repeated four times and four plants were infiltrated by each VIGS construct in every VIGS experiment. Plants infiltrated by the same VIGS construct showed similar morphological phenotypes, which were consistent in every VIGS experiment.

Semi-Quantitative RT–PCR Analysis

Total RNA was extracted from the stems containing one to seven internodes of 3-wpi VIGS plants using the RNeasy plant minikit (Qiagen). First-strand cDNA was synthesized using 2 μg of total RNA and SuperScript reverse transcriptase (Invitrogen). The transcripts of *NbCesA6*, *NbCesA8*, *NbCOBRA*, *NbIRX8*, *NbIRX9*, *NbIRX14*, *NbCOMT*, *NbCCR*, and *Nb4CL* were examined using gene-specific primers (Supplemental Table 1).

Microscopic Image analysis

Stem internodes of VIGS plants were fixed in Formalin–acetic acid–alcohol (FAA) solution. After fixation, internodes were dehydrated through a gradient of ethanol and finally embedded in wax. Five-micrometer-thick sections were cut with a -microtome. Three successive sections with the interval of 200 μm were mounted on one slide. De-waxed sections were stained with Toludine Blue O (TBO) for collecting images using a light microscope. For localization of cellulose, sections were incubated with His-tagged recombinant protein CBM3a (PlantProbes) that binds to crystalline cellulose (Blake et al., 2006) and then incubated with anti-His tag antibody (Sigma). Immunolocalizations of xylan and xyloglucan were carried out using the LM10 and LM15 monoclonal antibodies (PlantProbes) that recognize unsubstituted and relatively low-substituted xylans (McCartney et al., 2005) and the XXXG motif of xyloglucan (Marcus et al., 2008), respectively, followed by incubation with fluorescein isothiocyanate (FITC)-conjugated secondary antibody (Sigma). The FITC fluorescence-labeled sections and UV-illuminated sections were observed under a Zeiss Axiovert 200 M inverted microscope equipped with an AxioCam fluorescence camera. FITC fluorescence images and UV-induced autofluorescence images of VIGS and the control plants were captured under the same microscope and camera settings.

Cellulose and Xylan CoMPP Arrays

A sequential extraction of cellulose and xylan from the stems containing the first to seventh internodes of 3-wpi VIGS plants was performed using the method described previously (Moller et al., 2007). Two microliter extracts were spotted on the nitrocellulose membrane. The printed membranes were dried overnight and blotted on Western blotting buffer (LI-COR). His-tagged recombinant protein CBM3a and primary antibody LM10, in conjunction with anti-His tag antibody and/or IRDye 800CW (LI-COR) secondary antibodies, were used to probe microcrystalline cellulose and xylan on the dot-blotted membranes, respectively. Infrared images of membrane blots were scanned and analyzed by the Odyssey® Infrared Imaging System.

Cell Wall Alcohol Insoluble Residue (AIR) Fractionation

Cell walls (AIR) were subjected to sequential extraction with increasingly harsh reagents in order to isolate fractions enriched in various cell wall components. All extractions were carried out in suspensions at 10 mg mL^{-1} based on the starting weight of the AIR used. The AIR was first suspended in 50 mM ammonium oxalate (pH 5.0) and incubated overnight at room temperature with constant mixing. After the incubation, the solid residue was pelleted by centrifugation at 3400 *g* and the supernatant decanted and saved. The pellet was re-suspended in the same volume of de-ionized water, pelleted again as before, and the supernatant decanted and discarded. The pellet was then sequentially extracted in the same manner using 50 mM sodium carbonate (pH 10), 1 M KOH and 4 M KOH. The residual pellet from the 4 M KOH extraction was treated with sodium chlorite (100 mM) (Ahlgren and Goring, 1971) to break down the lignin polymers into small fragments. Finally, the pelleted chlorite residue was treated once more with 4 M KOH to isolate material that had been held in the walls by lignin (4 M KOHPC). The residual pellet was not further analyzed. All of the extracts were dialyzed against four changes of 4 L of de-ionized water and then lyophilized.

Total Sugar Estimation and ELISA

All cell wall extracts were dissolved in de-ionized water at 0.2 mg mL^{-1}. Total sugar contents of cell wall extracts were

Downloaded from mplant.oxfordjournals.org at Oak Ridge National Lab/UT-Battelle on September 14, 2011

estimated using the phenol–sulfuric acid method (Masuko et al., 2005) and all extracts were diluted to the same sugar concentration for loading onto the ELISA plates. Cell wall extracts (60 μg sugar mL^{-1}) were applied to the wells of ELISA plates (Costar 3598) at 50 μL per well and allowed to evaporate to dryness overnight at 37°C. ELISAs were performed as described (Pattathil et al., 2010), using a series of 150 monoclonal antibodies directed against plant cell wall carbohydrate epitopes (Pattathil et al., 2010). ELISA data are presented as a heat map in which the antibody order is based on a hierarchical clustering analysis of the antibody collection that groups the antibodies based on their binding to a panel of diverse plant glycans (Pattathil et al., 2010).

Monoclonal Antibodies

Monoclonal antibodies were obtained as hybridoma cell culture supernatants either from laboratory stocks at the Complex Carbohydrate Research Center [CCRC, JIM and MAC series; available from CarboSource Services (www.carbosource.net)], or from Plant Probes [LM series, PAM1; (www.plantprobes.net)].

SUPPLEMENTARY DATA

Supplementary Data are available at *Molecular Plant Online.*

FUNDING

The financial support provided by the NSF CAREER program (IBN-0236492), USDA-NRI program (2005–35103–15256), and CPBR funding (G012026–269) to C.P.J. is gratefully acknowledged. This work was also partially supported by the World Class University project of the Ministry of Science and Technology of Korea (R31-2009-000-20025-0). Generation of the CCRC-series of monoclonal antibodies used in this research was supported by a grant from the NSF Plant Genome Program (DBI-0421683) to M.G.H. Work in the Hahn laboratory on glycome profiling is supported by the US Department of Energy (BioEnergy Science Center and grant DE-PS02-06ER64304). The BioEnergy Science Center is a US Department of Energy Bioenergy Research Center supported by the Office of Biological and Environmental Research in the DOE Office of Science.

ACKNOWLEDGMENTS

We thank Dr Ryan J. Gilbert for providing assistance in the microscopic work. No conflict of interest declared.

REFERENCES

Ahlgren, P.A., and Goring, D.A.I. (1971). Removal of wood components during chlorite delignification of black spruce. Canadian J. Chem. **49,** 1272–1275.

Anterola, A.M., and Lewis, N.G. (2002). Trends in lignin modification: a comprehensive analysis of the effects of genetic manipulations/mutations on lignification and vascular integrity. Phytochemistry. **61,** 221–294.

Aspeborg, H., et al. (2005). Carbohydrate-active enzymes involved in the secondary cell wall biogenesis in hybrid aspen. Plant Physiol. **137,** 983–997.

Atanassova, R., Favet, N., Martz, F., Chabbert, B., Tollier, M.T., Monties, B., Fritig, B., and Legrand, M. (1995). Altered lignin composition in transgenic tobacco expressing O-methyltransferase sequences in sense and antisense orientation. Plant J. **8,** 465–477.

Baskin, T.I. (2005). Anisotropic expansion of the plant cell wall. Annu. Rev. Cell Dev. Biol. **21,** 203–222.

Baucher, M., El Jaziri, M., and Vandeputte, O. (2007). From primary to secondary growth: origin and development of the vascular system. J. Exp. Bot. **58,** 3485–3501.

Blake, A.W., McCartney, L., Flint, J.E., Bolam, D.N., Boraston, A.B., Gilbert, H.J., and Knox, J.P. (2006). Understanding the biological rationale for the diversity of cellulose-directed carbohydrate-binding modules in prokaryotic enzymes. J. Biol. Chem. **281,** 29321–29329.

Boerjan, W., Ralph, J., and Baucher, M. (2003). Lignin biosynthesis. Annu. Rev. Plant Biol. **54,** 519–546.

Brown, D.M., Goubet, F., Wong, V.W., Goodacre, R., Stephens, E., Dupree, P., and Turner, S.R. (2007). Comparison of five xylan synthesis mutants reveals new insight into the mechanisms of xylan synthesis. Plant J. **52,** 1154–1168.

Brown, D.M., Zeef, L.A., Ellis, J., Goodacre, R., and Turner, S.R. (2005). Identification of novel genes in *Arabidopsis* involved in secondary cell wall formation using expression profiling and reverse genetics. Plant Cell. **17,** 2281–2295.

Burch-Smith, T.M., Anderson, J.C., Martin, G.B., and Dinesh-Kumar, S.P. (2004). Applications and advantages of virus-induced gene silencing for gene function studies in plants. Plant J. **39,** 734–746.

Burton, R.A., Gibeaut, D.M., Bacic, A., Findlay, K., Roberts, K., Hamilton, A., Baulcombe, D.C., and Fincher, G.B. (2000). Virus-induced silencing of a plant cellulose synthase gene. Plant Cell. **12,** 691–706.

Chabannes, M., Barakate, A., Lapierre, C., Marita, J.M., Ralph, J., Pean, M., Danoun, S., Halpin, C., Grima-Pettenati, J., and Boudet, A.M. (2001). Strong decrease in lignin content without significant alteration of plant development is induced by simultaneous down-regulation of cinnamoyl CoA reductase (CCR) and cinnamyl alcohol dehydrogenase (CAD) in tobacco plants. Plant J. **28,** 257–270.

Ching, A., Dhugga, K.S., Appenzeller, L., Meeley, R., Bourett, T.M., Howard, R.J., and Rafalski, A. (2006). Brittle stalk 2 encodes a putative glycosylphosphatidylinositol-anchored protein that affects mechanical strength of maize tissues by altering the composition and structure of secondary cell walls. Planta. **224,** 1174–1184.

Cosgrove, D.J. (2005). Growth of the plant cell wall. Nat. Rev. Mol. Cell Biol. **6,** 850–861.

Dong, Y., Burch-Smith, T.M., Liu, Y., Mamillapalli, P., and Dinesh-Kumar, S.P. (2007). A ligation-independent cloning tobacco rattle virus vector for high-throughput virus-induced gene silencing identifies roles for NbMADS4-1 and –2 in floral development. Plant Physiol. **145,** 1161–1170.

Fagard, M., Desnos, T., Desprez, T., Goubet, F., Refregier, G., Mouille, G., McCann, M., Rayon, C., Vernhettes, S., and Hofte, H. (2000). PROCUSTE1 encodes a cellulose synthase required for normal cell elongation specifically in roots and dark-grown hypocotyls of *Arabidopsis*. Plant Cell. **12,** 2409–2424.

Farrokhi, N., Burton, R.A., Brownfield, L., Hrmova, M., Wilson, S.M., Bacic, A., and Fincher, G.B. (2006). Plant cell wall biosynthesis:

Downloaded from mplant.oxfordjournals.org at Oak Ridge National Lab/UT-Battelle on September 14, 2011

genetic, biochemical and functional genomics approaches to the identification of key genes. Plant Biotechnol. J. **4,** 145–167.

Joshi, C.P., Bhandari, S., Ranjan, P., Kalluri, U.C., Liang, X., Fujino, T., and Samuga, A. (2004). Genomics of cellulose biosynthesis in poplars. New Phytologist. **164,** 53–61.

Kajita, S., Mashino, Y., Nishikubo, N., Katayama, Y., and Omori, S. (1997). Immunological characterization of transgenic tobacco plants with a chimeric gene for 4-coumarate:CoA ligase that have altered lignin in their xylem tissue. Plant Science. **128,** 109–118.

Ko, J.H., Kim, J.H., Jayanty, S.S., Howe, G.A., and Han, K.H. (2006). Loss of function of COBRA, a determinant of oriented cell expansion, invokes cellular defence responses in *Arabidopsis thaliana*. J. Exp. Bot. **57,** 2923–2936.

Lagaert, S., BeliÎn, T., and Volckaert, G. (2009). Plant cell walls: protecting the barrier from degradation by microbial enzymes. Seminars in Cell & Developmental Biology. **20,** 1064–1073.

Li, Y., et al. (2003). BRITTLE CULM1, which encodes a COBRA-like protein, affects the mechanical properties of rice plants. Plant Cell. **15,** 2020–2031.

Liu, Y., Schiff, M., Marathe, R., and Dinesh-Kumar, S.P. (2002). Tobacco Rar1, EDS1 and NPR1/NIM1 like genes are required for N-mediated resistance to tobacco mosaic virus. Plant J. **30,** 415–429.

Lu, R., Martin-Hernandez, A.M., Peart, J.R., Malcuit, I., and Baulcombe, D.C. (2003). Virus-induced gene silencing in plants. Methods. **30,** 296–303.

Marcus, S., Verhertbruggen, Y., Herve, C., Ordaz-Ortiz, J., Farkas, V., Pedersen, H., Willats, W., and Knox, J.P. (2008). Pectic homogalacturonan masks abundant sets of xyloglucan epitopes in plant cell walls. BMC Plant Biology. **8,** 60.

Masuko, T., Minami, A., Iwasaki, N., Majima, T., Nishimura, S.I., and Lee, Y.C. (2005). Carbohydrate analysis by a phenol-sulphuric acid method in microplate format. Anal. Biochem. **339,** 69–72.

McCartney, L., Marcus, S.E., and Knox, J.P. (2005). Monoclonal antibodies to plant cell wall xylans and arabinoxylans. J. Histochem. Cytochem. **53,** 543–546.

Mellerowicz, E.J., Baucher, M., Sundberg, B., and Boerjan, W. (2001). Unravelling cell wall formation in the woody dicot stem. Plant Mol. Biol. **47,** 239–274.

Mohnen, D., Bar-Peled, M., and Somerville, C. (2008). Cell wall polysaccharide synthesis. In Biomass Recalcitrance: Deconstructing the Plant Cell Wall for Bioenergy, Himmel D.E., ed. (Oxford, UK: Blackwell Publishing Ltd), pp. 94–187.

Moller, I., et al. (2007). High-throughput mapping of cell-wall polymers within and between plants using novel microarrays. Plant J. **50,** 1118–1128.

Ni, W., Paiva, N.L., and Dixon, R.A. (1994). Reduced lignin in transgenic plants containing a caffeic acid O-methyltransferase antisense gene. Transgenic Research. **3,** 120–126.

Pattathil, S., et al. (2010). A comprehensive toolkit of plant cell wall glycan-directed monoclonal antibodies. Plant Physiol. April. **2,** 10.1104/pp.109.151985.

Pauly, M., and Keegstra, K. (2008). Cell-wall carbohydrates and their modification as a resource for biofuels. Plant J. **54,** 559–568.

Peña, M.J., Zhong, R., Zhou, G.K., Richardson, E.A., O'Neill, M.A.A., Darvil, G., York, W.S., and Ye, Z.H. (2007). *Arabidopsis irregular xylem8* and *irregular xylem9*: Implications for the complexity of glucuronoxylan biosynthesis. Plant Cell. **19,** 549–563.

Persson, S., Wei, H., Milne, J., Page, G.P., and Somerville, C.R. (2005). Identification of genes required for cellulose synthesis by regression analysis of public microarray data sets. Proc. Natl Acad. Sci. U S A. **102,** 8633–8638.

Piquemal, J., Lapierre, C., Myton, K., O'Connell, A., Schuch, W., Grima-Pettenati, J., and Boudet, A.M. (1998). Downregulation of cinnamoyl-CoA reductase induces significant changes of lignin profiles in transgenic tobacco plants. Plant J. **13,** 71–83.

Robertson, D. (2004). VIGS vectors for gene silencing: many targets, many tools. Annu. Rev. Plant Biol. **55,** 495–519.

Roudier, F., et al. (2005). COBRA, an *Arabidopsis* extracellular glycosyl-phosphatidyl inositol-anchored protein, specifically controls highly anisotropic expansion through its involvement in cellulose microfibril orientation. Plant Cell. **17,** 1749–1763.

Sandhu, A.P.S., Randhawa, G.S., and Dhugga, K.S. (2009). Plant cell wall matrix polysaccharide biosynthesis. Mol. Plant. **2,** 840–850.

Schindelman, G., Morikami, A., Jung, J., Baskin, T.I., Carpita, N.C., Derbyshire, P., McCann, M.C., and Benfey, P.N. (2001). COBRA encodes a putative GPI-anchored protein, which is polarly localized and necessary for oriented cell expansion in *Arabidopsis*. Genes Dev. **15,** 1115–1127.

Somerville, C. (2006). Cellulose synthesis in higher plants. Annu. Rev. Cell Dev. Biol. **22,** 53–78.

Sterky, F., et al. (1998). Gene discovery in the wood-forming tissues of poplar: analysis of 5, 692 expressed sequence tags. Proc. Natl Acad. Sci. U S A. **95,** 13330–13335.

Sterky, F., et al. (2004). A *Populus* EST resource for plant functional genomics. Proc. Natl Acad. Sci. U S A. **101,** 13951–13956.

Stone, B.A., Evans, N.A., Bonig, I., and Clarke, A.E. (1984). The application of Sirofluor, a chemically defined fluorochrome from aniline blue for the histochemical detection of callose. Protoplasma. **122,** 191–195.

Taylor, N.G., Laurie, S., and Turner, S.R. (2000). Multiple cellulose synthase catalytic subunits are required for cellulose synthesis in *Arabidopsis*. Plant Cell. **12,** 2529–2540.

Wood, P.J., Fulcher, R.G., and Stone, B.A. (1983). Studies on the specificity of interaction of cereal cell wall components with Congo red and Calcofluor: specific detection and histochemistry of (1,3), (1,4)-β-D-glucan. J. Cereal Sci. **1,** 95–110.

Yong, W., et al. (2005). Genomics of plant cell wall biogenesis. Planta. **221,** 747–751.

York, W.S., and O'Neill, M.A. (2008). Biochemical control of xylan biosynthesis: which end is up? Curr. Opin. Plant Biol. **11,** 258–265.

Zhong, R., Morrison, W.H.III, Negrel, J., and Ye, Z.H. (1998). Dual methylation pathways in lignin biosynthesis. Plant Cell. **10,** 2033–2045.

Zhu, X., and Dinesh-Kumar, S.P. (2008a). Virus-induced gene silencing as a tool to identify host genes affecting viral pathogenicity. Methods Mol. Biol. **451,** 641–648.

Zhu, X., and Dinesh-Kumar, S.P. (2008b). Virus-induced gene silencing (VIGS) to study gene function in plants. RNA Interference. In Methods for Plants and Animals, Doran T. and Helliwell C., eds : (Wallingford: CABI Publishing), pp. 26–49.

Downloaded from mplant.oxfordjournals.org at Oak Ridge National Lab/UT-Battelle on September 14, 2011